European ECOSTRESS Hub Validation Report

Reference: EEH-D6-VR

ESA Contract No. 4000129873/20/I-NS

Prepared by	Tian Hu, Kaniska Mallick, Patrik Hitzelberger, Yoanne Didry and Martin Schlerf (LIST)
Reference	EEH-D6-VR
Issue	1
Revision	0
Date of Issue	2022-06-22
Status	**Draft**
Document Type	Validation Report
Distribution	LIST, ESA

DISTRIBUTION LIST

Name	Affiliation
Zoltan Szantoi	ESA (TO)
Kaniska Mallick	LIST (PI)
Patrik Hitzelberger	LIST (co-PI)
Martin Schlerf	LIST
Yoanne Didry	LIST
Tian Hu	LIST

APPROVAL

Name	Affiliation	Date	Signature
Zoltan Szantoi	ESA (TO)		

CHANGE LOG

Issue	Revision	Date	Author	Comment
1	0	2022-06-22	Hu, Mallick, Hitzelberger, Didry, Schlerf	Initial version

Contents

Abstract

Land surface temperature (LST) and evapotranspiration (ET) are important variables in the surface energy and water balance, playing a dominant role in biophysical interactions between the terrestrial ecosystems and the atmosphere. In the European ECOSTRESS Hub (EEH), the target is to produce LST and ET products from the ECOSTRESS data with high spatial (~70 m) and moderate temporal (3--5 day) resolutions on a cloud computing system over Europe and Africa. The LST data are produced from two widely used algorithms, i.e., Temperature and Emissivity Separation (TES) and Split-Window (SW). With regard to the ET data, three structurally different models are employed, including the one-source non-parametric Surface Temperature Initiated Closure (STIC) model, the one-source parametric Surface Energy Balance System (SEBS) model and the two-source parametric Two-Source Energy Balance (TSEB) model.

EEH provides an opportunity for a comprehensive comparison between different LST algorithms and ET models at the continent scale. In the evaluation, the EEHSW and EEHTES LST data were compared with the official ECOSTRESS LST data produced by NASA/JPL at nine sites with different land surface types over Europe and Africa for the period between August 2018 and December 2021. The three ET datasets produced in the EEH were evaluated using the flux measurements at eighteen eddy covariance (EC) sites distributed in regions with different aridity levels over Europe for the period between August 2018 and December 2019. Additionally, the STIC ET data were compared with the official ECOSTRESS ET (PT-JPL) data at the same EC sites for the period between August 2018 and December 2021.

1. EEH products

In the period from August 2018 to December 2019, two LST and three ET datasets are produced for a comprehensive evaluation of algorithms and models in the EEH. After this period, both the LST datasets will continue to be produced. Whereas, the precalculated ET datasets for the entire ECOSTRESS acquisition span will only be produced from the STIC model. All these data will be accessible to the public and free to download from the Food Security Thematic Exploitation Platform (FS-TEP). The specifics of data availability are described in Table 1.1 below. More detail regarding the two LST estimation algorithms and three ET estimation models can be found in the accompanying ATBD documents.

Table 1.1. Data availability in the EEH

Data	Algorithm/model	Available period	Notes
LST	TES	2018.08-2021.12	Produced for the entire period
LST	SW	2018.08-2021.12	Emissivity is estimated using bare soil emissivity from the ASTER GED data and vegetation information from the Copernicus Global Land Service
ET	STIC	2018.08-2021.12	Produced for the entire period
ET	TSEB	2018.08-2019.12	n/a
ET	SEBS	2018.08-2019.12	n/a

To mitigate the impacts of cloud contamination, a clear-sky conservative cloud mask product is produced together with LST and ET data. In the evaluation, only clear-sky pixels after cloud screening are used to avoid abnormal values due to the cloud influence.

2. LST evaluation

Two different algorithms are used to obtain LST in the EEH, i.e., the TES and the SW methods. In the TES algorithm, temperature and emissivity are retrieved simultaneously in an iterative method. Whereas, in the SW algorithm, emissivity is estimated first based on the bare soil emissivity extracted from the ASTER GED data and then adjusted using vegetation and snow coverage data. Taking advantage of the prior emissivity information, LST is obtained through an empirical equation.

2.1. Evaluation method

2.1.1. T-based validation

In this study, the T-based validation strategy was adopted for the LST evaluation. The different LST products were compared with *in-situ* measurements for the period between August 1, 2018 and December 31, 2021 over Europe and Africa. To mitigate cloud contamination, only pixels surrounded by 15 × 15 (approximately 1 km × 1 km) cloud-free pixels were used in the evaluation. This is particularly important for ECOSTRESS LST validation since the cloud mask was generated using only the TIR bands available. Meanwhile, the “3σ-Hampel identifier” was adopted to remove the outliers caused by cloud contamination or other radiance-related issue. The standard deviation used in the method is calculated as follows

$$S = 1.4826 \times \mathrm{median}(|x_i - x_m|) \quad (2.1)$$

where S is the standard deviation, x_i is the difference between the LST retrieval and *in-situ* measurement, x_m is the median of the difference. LST retrievals with LST differences below x_m-$3S$ or above x_m+$3S$ were regarded as outliers and excluded from the evaluation.

The footprint of a radiometer on the ground normally covers an area with a radius between 1 and 10 m. For a pyrgeometer, the radius of the footprint is between 10 and 100 m. The ground footprints of the measurements against the spatial resolutions of LST products are important for the evaluation results. To ensure the spatial representativeness of the *in-situ* measurements, only match-ups with a standard deviation <1 K within a 3 × 3 window centered

on the sites were retained. To account for the geo-registration uncertainty in ECOSTRESS data, the ECOSTRESS LST data within the 3 × 3 window were averaged for use in the evaluation.

Three indices were used to quantify the performance of these LST products based on the recommendation by the Committee on Earth Observation Satellites (CEOS) Working Group on Calibration and Validation - Land Product Validation (LPV) Subgroup (Guillevic et al. 2018). The total uncertainty is estimated via root-mean-square error (RMSE) as follows:

$$RMSE = \sqrt{\frac{\sum(LST_{sat} - LST_{insitu})^2}{N}} \quad (2.2)$$

where LST_{sat} and LST_{insitu} are the LST products and *in-situ* measurements, respectively, N is the sample number. The accuracy is estimated via bias μ as follows:

$$\mu = \text{median}\left(LST_{sat,i} - LST_{insitu,i}\right). \quad (2.3)$$

The median is used in lieu of the mean to avoid the impacts of outliers in statistics. Similarly, the median of the absolute residual is calculated as an estimate of the precision σ:

$$\sigma = 1.4826 \times \text{median}\left(\left|\left(LST_{sat,i} - LST_{insitu,i}\right) - \mu\right|\right). \quad (2.4)$$

Ground measurements from four different networks were used to evaluate the high spatial resolution LST, including the Karlsruhe Institute of Technology (KIT) network, the Baseline Surface Radiation Network (BSRN), the Global Change Unit (GCU) network and the Integrated Carbon Observation System (ICOS) network. The detailed information of these sites is listed in Table 2.1. The spatial distribution of the 9 sites is shown in Fig. 2.1.

Table 2.1 Information of the selected 9 *in-situ* measurement sites.

Site No.	Site location	Site ID	Network	Latitude	Longitude	Surface type	Emissivity
1	Gobabeb wind tower, Namibia	GBB	KIT	23.551° S	15.051° E	Barren/sparsely vegetated	0.940 Hulley et al. (2021)
2	Lake Constance, Germany	CNS	KIT	47.605° N	9.444° E	Water	0.973 Hulley et al. (2021)
3	KIT Forest, Germany	KIT	KIT	49.091° N	8.425° E	Mixed forest	0.988 Freitas et al. (2009)
4	Cabauw, Netherlands	CAB	BSRN	51.971° N	4.927° E	Grassland	From ECOSTRESS Measurements
5	Fuente Duque, Donana, Spain	FDU	GCU	36.998° N	6.434° W	Marshland	Sobrino and Skoković (2016)

6	Balsa Blanca, Cabo de Gata, Spain	CDG	GCU	36.939° N	2.034° W	Woody savannas	Measurements Sobrino and Skoković (2016)
7	Fontainebleau-Barbeau, France	FON	ICOS	48.476° N	2.780° E	Deciduous broadleaf forest	From ECOSTRESS
8	Lison, Italy	LSN	ICOS	45.740° N	12.750° E	Cropland	From ECOSTRESS
9	San Rossore 2, Italy	SR2	ICOS	43.732° N	10.291° E	Evergreen needleleaf forest	From ECOSTRESS

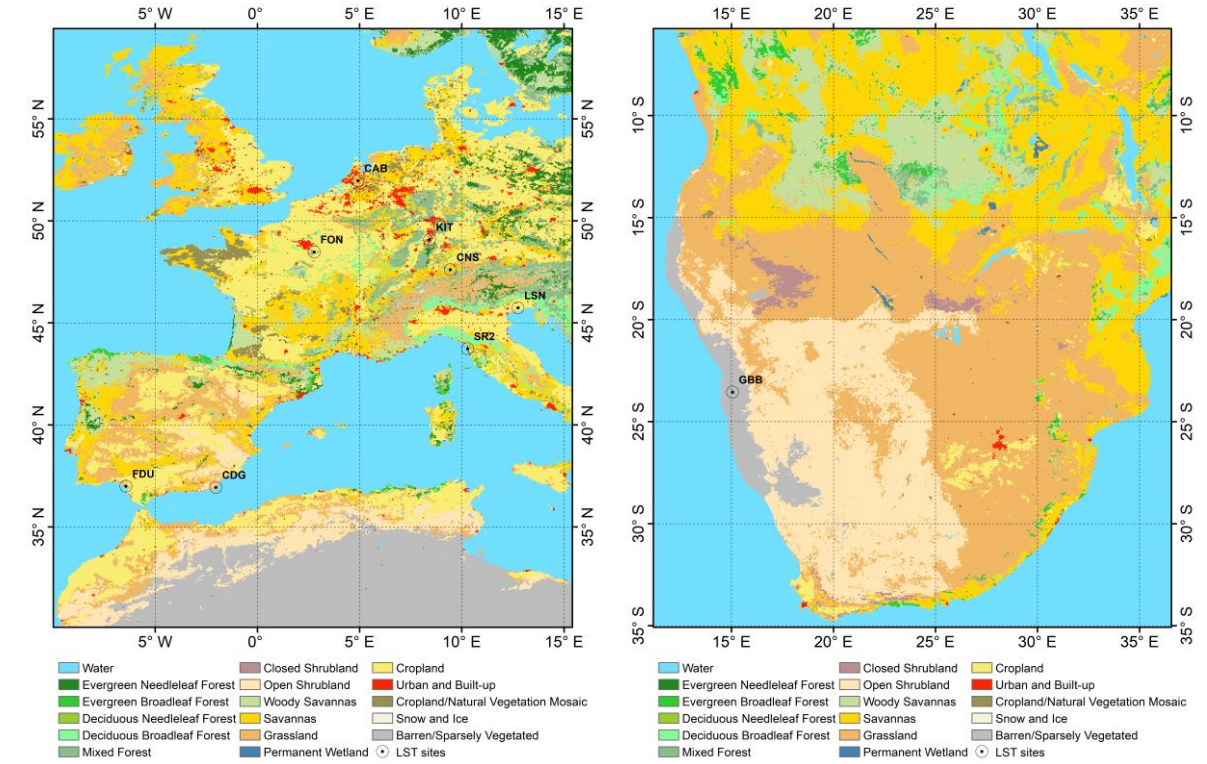

Fig. 2.1 Spatial distribution of the nine *in-situ* measurement sites, including 8 sites over Europe and 1 site over Africa.

The KIT stations were designed to validate LST over relatively homogeneous surfaces. The surface upwelling and downwelling radiances are collected using narrow-band radiometers measuring TIR radiance between 9.6 and 11.5 µm (Göttsche et al. 2016). The radiometers are mounted at heights between 12 and 28 m and measure the radiances once per minute, which results in fields of view (FOV) between 3 and 14 m^2. Three KIT sites over desert, water surface and mixed forest were selected.

The BSRN was set up to provide observations of the best possible quality for short- and long-wave surface radiation fluxes sampled at high frequency (once per minute). The measurements from well calibrated pyrgeometers are expected to provide reference for the

validation of satellite-based estimates of the surface radiative fluxes and for the comparison to climate model calculations (Driemel et al. 2018). Here, only one BSRN site CAB was selected considering both upwelling and downwelling radiation fluxes are collected at this site and the accuracy of the measurements has been demonstrated in the previous studies (Trigo et al. 2021).

The GCU sites were set up in Spain for the calibration of TIR sensors and the validation of satellite LST products (Sobrino and Skoković 2016). Thermal radiance measurements are collected for the spectral range between 8 and 14 μm. The measurements are collected every 10 s and averaged to 5 min. Two permanent sites providing long-term observations were selected from the GCU sites.

The ICOS network was developed to produce standardized, high-precision and long-term observations for understanding the carbon cycle and providing necessary information on greenhouse gases. The ICOS sites measure the fluxes of greenhouse gases, living and non-living components as well as drivers (e.g., radiations) for the exchange of greenhouse gases, water and energy between ecosystems and the atmosphere. We selected five sites over different land surface types. The upwelling and downwelling radiations are measured using pyrgeometers and averaged for each half hour.

Estimating LST from the radiance measurements of the KIT and GCU sites was achieved by inverting the Planck's law as follows:

$$B_i(T_s) = \frac{L_{up,i} - (1 - \varepsilon_i)L_{down,i}}{\varepsilon_i} \quad (2.5)$$

where $L_{up,i}$ is the upwelling longwave radiance measured by the station radiometers, $L_{down,i}$ is the downwelling thermal radiance, which is measured by an additional radiometer for the KIT sites and calculated by inputting MOD07 atmospheric profiles into the MODTRAN model, $\boldsymbol{\varepsilon_i}$ is the narrow-band emissivity, T_s is the inverted temperature. The band-effective emissivity was obtained using the methods listed in Table 2.1.

For the longwave radiation measurements from the BSRN and ICOS sites, the LST is estimated by inverting the Stefan-Boltzmann's law as follows:

$$T_s = \sqrt[4]{\frac{R_{up} - (1 - \varepsilon_{BB})R_{down}}{\varepsilon_{BB}\sigma}} \quad (2.6)$$

where R_{up} and R_{down} are the measured upward and downward longwave radiations, respectively, ε_{BB} is the broadband emissivity and σ is the Stefan-Boltzmann constant. The broadband emissivity was estimated from the ECOSTRESS emissivity retrievals in the three thermal bands as follows:

$$\varepsilon_{BB} = 0.3287\varepsilon_2 + 0.3783\varepsilon_4 + 0.3158\varepsilon_5 - 0.0255 \quad (2.7)$$

where ε_2, ε_4 and ε_5 are the emissivity retrievals in bands 2, 4 and 5, respectively.

2.1.2. Cross-satellite validation

The Landsat and Terra carrying ASTER have sun-synchronous orbits. This feature leads to a fixed overpass time, which is around 10 a.m. for Landsat and 10: 30 a.m./p.m. for ASTER. Due to the asynchronous orbits of ISS, the overpass time of ECOSTRESS is variant. It is therefore challenging to obtain concurrent Landsat and ASTER LST with the ECOSTRESS LST. In this case, the Landsat and ASTER LST retrievals were evaluated for the same period at the 9 selected ground sites, and the same accuracy indicators were used as mentioned in Eqs. 2.2−2.4.

2.2. LST evaluation results

2.2.1. Evaluation results using in-situ measurements

Fig. 2.2 shows the evaluation results of ECOSTRESS LST at the 9 sites. The sample numbers are above 15 at most sites except for the 2 GCU sites. The RMSE of the three ECOSTRESS LST are below 3 K and μ (absolute value) are within 2 K at most sites except for the two ICOS sites FON and LSN. The performances of LST retrievals at GBB, CNS, KIT and CGD are better as compared to the other sites. The RMSE are below 2 K and μ (absolute value) are around 1 K at these 4 sites. This could be attributed to the homogeneous landscape at these sites and that radiance measurements are collected by radiometers instead of radiation fluxes by pyrgeometers. The unsatisfying performances at the ICOS sites could be because of the half hour sampling frequency that is too sparse for LST validation.

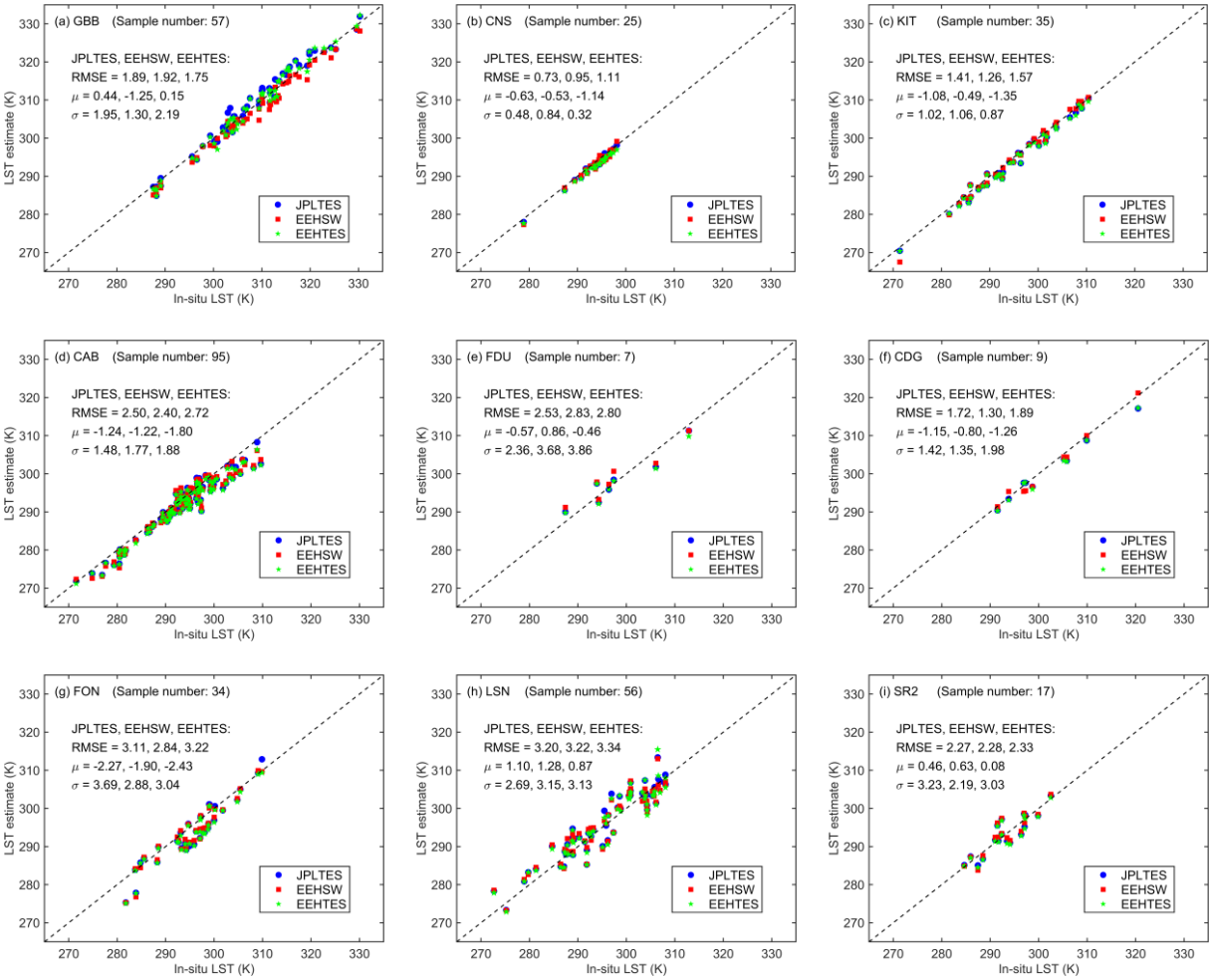

Fig. 2.2 ECOSTRESS LST against in-situ measurements (K) at the nine ground sites.

Overall, the three ECOSTRESS LST are very close, with a difference of RMSE within 0.2 K (Fig. 2.3). The EEHSW LST has the lowest RMSE and σ while the JPLTES LST has the lowest μ (absolute value). The RMSE obtained using all the 9 sites for the three LST are ~2.4 K, while the RMSE is reduced to approximately 2 K by using the 6 sites with fine sampling frequencies. A cold bias exists for all the three LST, which is more pronounced for LST below 295 K. This agrees well with the finding by Hulley et al. (2021) and relates to the radiometric calibration of the ECOSTRESS radiance data.

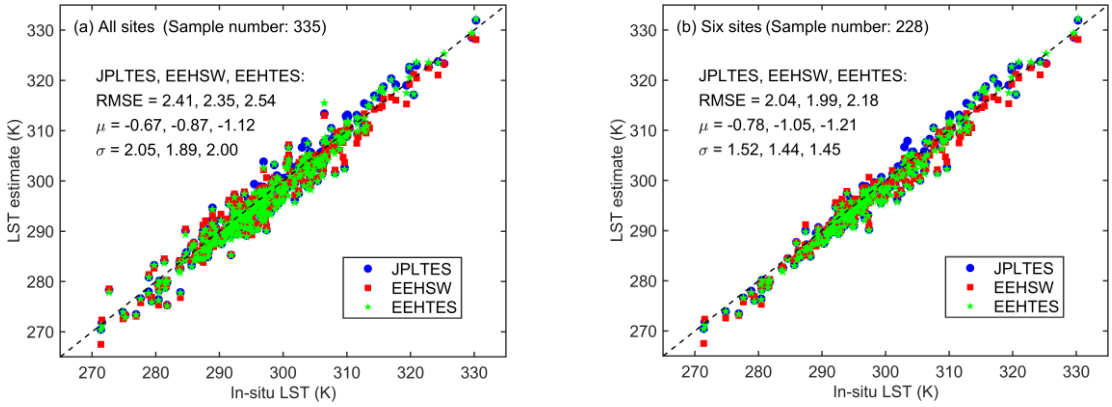

Fig. 2.3 ECOSTRESS LST retrievals vs. in-situ LST by assembling the samples (a) at all the sites and (b) at the 6 sites GBB, CNS, KIT, CAB, FUD and CDG.

2.2.2. Inter-comparison with Landsat and ASTER LST retrievals

The validation result of Landsat LST by gathering the samples at all sites is very close to that of ECOSTRESS LST (Fig. 2.4). The RMSE is 2.48 K using all the nine sites, with a difference from the three ECOSTRESS LST within 0.2 K. μ (absolute value, ~0.9 K) of Landsat LST is very close to those of the three LST. The RMSE obtained using the 6 sites is 2.2 K, which is slightly higher than those of the three ECOSTRESS LST.

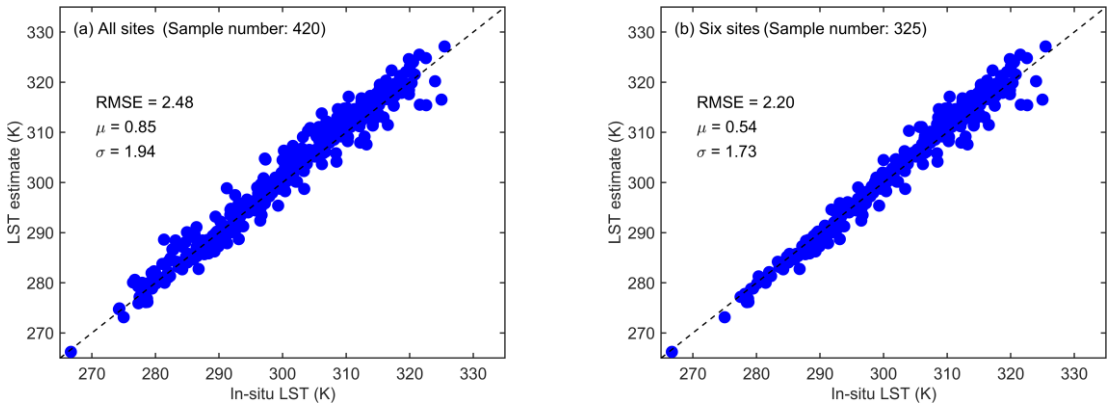

Fig. 2.4 Landsat LST against in-situ measurements (K) at the ground sites.

The ASTER LST have sparse coverages at most of the nine sites except for the site GBB, at which the sample number is above 10 (Fig. 2.5). At GBB, the RMSE (2 K) of ASTER LST is slightly higher (~0.1 K) than the three ECOSTRESS LST. Overall, the RMSE of the ASTER LST is 2.06 K using all the sites, which is around 0.4 K lower than the ECOSTRESS and Landsat LST. μ (absolute value) is close to the ECOSTRESS and Landsat LST, which is approximately 1 K. The RMSE obtained at the six sites is close to those of the three ECOSTRESS LST, which is ~2 K.

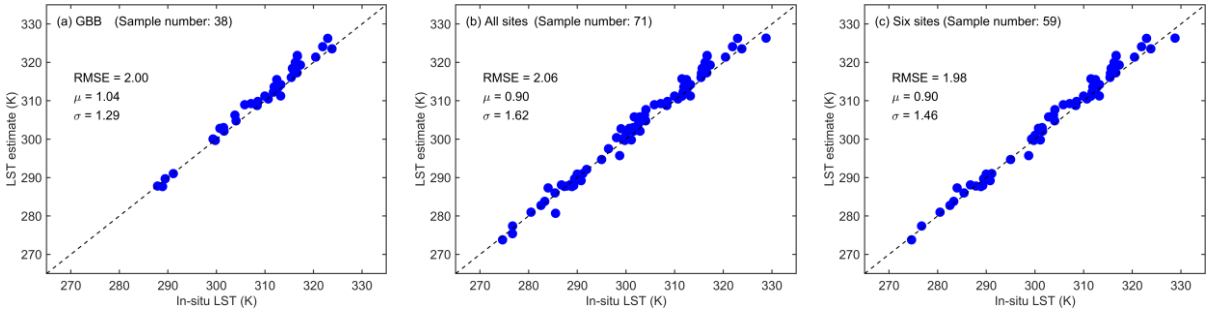

Fig. 2.5 ASTER LST against *in-situ* measurements (K) at (a) GBB and (b) all the 9 ground sites.

Among all the five LST retrievals (Fig. 2.6), the ASTER LST has the lowest RMSE when using all the sites. The JPL LST has the lowest μ (absolute value). σ of the ASTER LST is the smallest. When using the six sites (excluding ICOS sites), the JPLTES, EEHSW and ASTER LST have close RMSEs around 2 K, and the EEHTES and Landsat LST have slightly higher RMSEs around 2.2 K. In general, the five high spatial resolution LST retrievals show a high consistency, with RMSEs around 2 K, μ around 1 K and σ between 1 and 1.5 K.

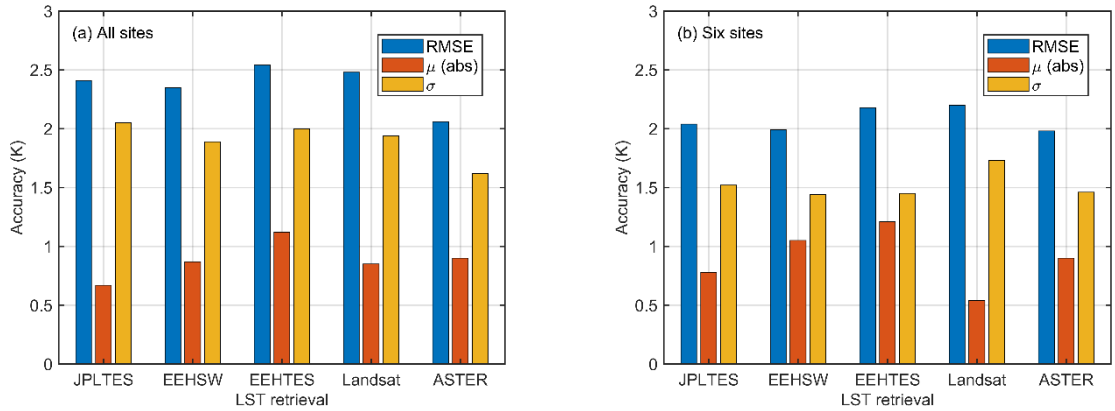

Fig. 2.6 Comparison among the five LST products in terms of RMSE, μ and σ for the nine sites. The absolute value of μ is shown and μ is negative for the JPL, EEHSW and EEHTES ECOSTRESS LST.

3. ET evaluation

Three ET models with different structures and conceptualizations are used in the EEH, i.e., STIC, TSEB and SEBS. STIC and SEBS are both one-source models, while TSEB is a two-source model that estimates transpiration and evaporation separately. These different ET estimates will be validated using heat flux measurements at the eddy covariance sites over different biomes.

3.1. Validation sites

To validate the EEH ET estimates, we selected a total of 18 sites from the European Fluxes Database Cluster (EFDC) and Integrated Carbon Observation System (ICOS) networks over different land cover types (Table 3.1). The ECOSTRESS instantaneous ET (in the form of latent heat flux, LE) retrieval will be compared directly to the 30 min instantaneous LE measurement. A detailed description of these sites is available on the EFDC (http://www.europe-fluxdata.eu/home/sites-list) and the ICOS (https://meta.icos-cp.eu/collections/Yljl66tHIJM-XlCmvTvMU3vi) websites.

Table 3.1 List of the selected eddy covariance flux sites. Biome is the IGBP classification, and climate is the Köppen climate type. Biomes covered in this study include deciduous broadleaf forest (DBF), evergreen needleleaf forest (ENF), mixed forest (MF), savanna (SAV), cropland (CRO), grassland (GRA), shrubland (SHR) and wetland (WET). Climate types include humid subtropical (Cfa), temperate oceanic (Cfb), hot-summer Mediterranean (Csa), hot-summer humid continental (Dfa), warm-summer humid continental (Dfb), and subacrtic (Dfc).

Site ID	Biome	Climate	Latitude (◦)	Longitude (◦)	Source
BE-Lcr	DBF	Cfb	51.11	3.85	ICOS
BE-Lon	CRO	Cfb	50.55	4.75	ICOS
BE-Maa	SHR	Cfb	50.98	5.63	ICOS
BE-Vie	MF	Cfb	50.31	6.00	EFDC
CZ-Wet	WET	Dfa	49.03	14.77	EFDC
DE-Geb	CRO	Cfb	51.10	10.92	EFDC
DE-Gri	GRA	Dfb	50.95	13.51	ICOS
DE-Kli	CRO	Dfb	50.89	13.52	EFDC
DE-Rur	GRA	Cfb	50.62	6.30	EFDC
DE-RuS	CRO	Dfb	50.87	6.45	ICOS
ES-LM1	SAV	Csa	39.94	-5.78	EFDC
FR-Aur	CRO	Cfb	43.55	1.11	ICOS
FR-Bil	ENF	Cfb	44.49	-0.96	ICOS
FR-Hes	DBF	Cfb	48.67	7.07	EFDC
FR-LGt	WET	Cfb	47.32	2.28	ICOS
FR-Mej	GRA	Cfb	48.12	-1.80	ICOS
IT-Lsn	SHR	Cfa	45.74	12.75	ICOS
IT-Tor	GRA	Dfc	45.84	7.58	ICOS

To ensure energy balance closure, the measured fluxes are adjusted based on the Bowen ratio

$$\beta = \frac{H}{\lambda E} \tag{3.1}$$

where β is the Bowen ratio, H is the sensible heat flux, λE is the latent heat flux. The correction items for H and λE are then calculated as

$$\Delta\lambda E = \frac{(RN - G) - (1 + \beta)\lambda E}{1 + \beta} \tag{3.2}$$

$$\Delta H = \beta(\lambda E + \Delta\lambda E) - H \tag{3.3}$$

where $\Delta\lambda E$ and ΔH are the correction items for latent and sensible heat fluxes, respectively, RN is the net radiation, G is the soil heat flux. The corrected heat fluxes are obtained by adding the correction items to the measured fluxes.

The following set of statistical metrics were used to assess model performances

$$r = \frac{\sum_{i=1}^{n}(E_i - \bar{E})\,(O_i - \bar{O})}{\sqrt{\sum_{i=1}^{n}(E_i - \bar{E})^2}\sqrt{\sum_{i=1}^{n}(O_i - \bar{O})^2}} \tag{3.4}$$

$$RMSE = \sqrt{\sum_{i=1}^{n}\frac{(E_i - O_i)^2}{n}} \tag{3.5}$$

$$bias = \sum_{i=1}^{n}\frac{E_i - O_i}{n} \tag{3.6}$$

where r is the Pearson's correlation coefficient, $RMSE$ is root-mean-square error, $bias$ is the mean bias, between the model and measurements, n is the total number of data pairs. E_i and O_i are the model estimated and measured SEB fluxes and $\bar{O}$ is the average of measured values and $\bar{E}$ is the average of estimated values.

3.2. ET evaluation results

Six land surface types were covered by the EC sites, including forest, cropland, grassland, shrubland, wetland and savanna (Fig. 3.1). Overall, the STIC ET is close to the SEBS ET, with similar RMSE, bias and r except over savanna. Comparatively, the uncertainty of the TSEB ET is notably larger than the other two ET estimates. Over forest, cropland and shrubland, the STIC ET has the best performance, with the lowest RMSE. Over grassland and wetland, SEBS

has the best performance. Only over savanna does the TSEB model show advantage over the other two ET.

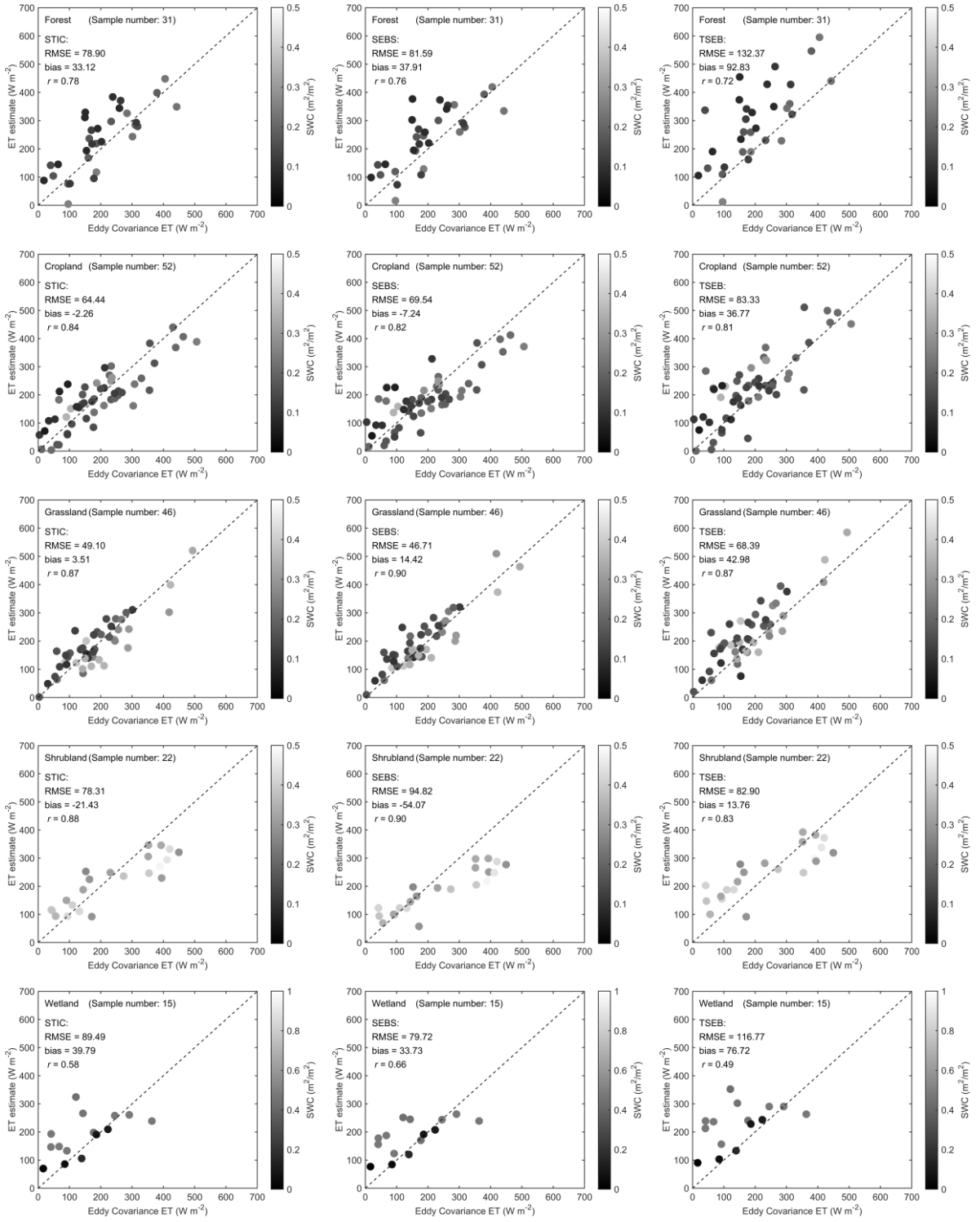

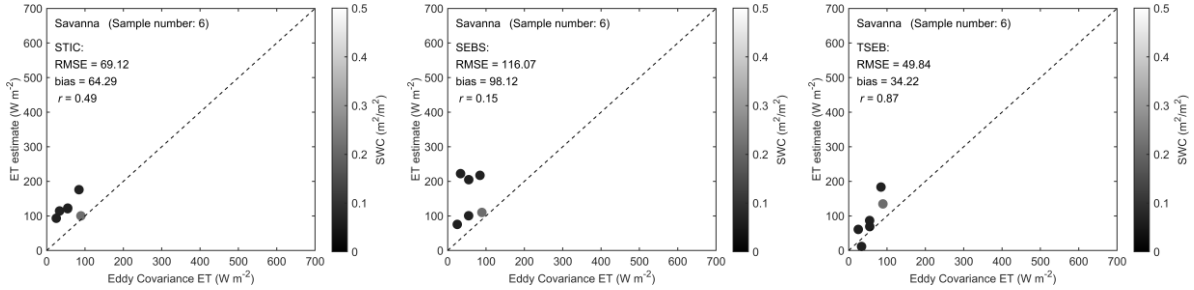

Fig. 3.1 Comparison between the observed ET at eddy covariance sites and instantaneous ET estimates from STIC, SEBS and TSEB for 6 land surface types during the period between 2018−2019.

The STIC ET has a RMSE of 68.35 W m^{-2}, a bias of 9.20 W m^{-2} and *r* of 0.81 over all the sites (Fig. 3.2). The SEBS ET is similar to the STIC ET, with a RMSE around 70 W m^{-2}, a bias within 10 W m^{-2} and *r* around 0.8. However, the RMSE of TSEB is obviously larger (~20 W m^{-2}) than those of the other two estimates, which is close to 95 W m^{-2}. Although the correlation with the EC measurements is good (with *r* close to 0.8), a systematic overestimation exists for the TSEB ET estimates, which is indicated in the large bias (~50 W m^{-2}).

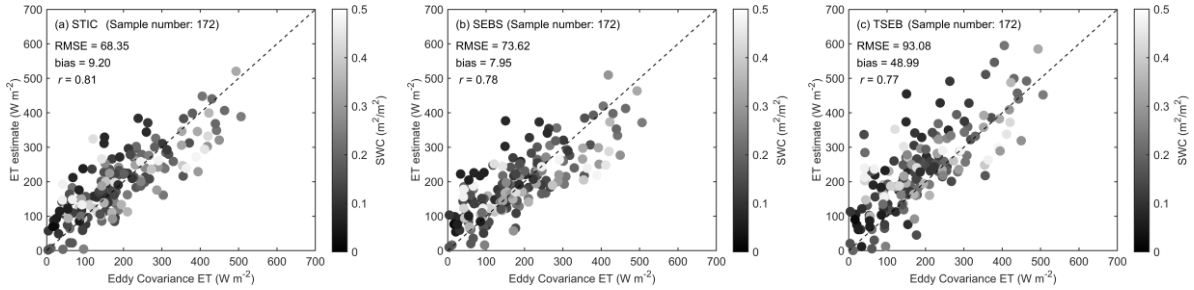

Fig. 3.2 Comparison between the observed ET and instantaneous ET estimates at all the eddy covariance sites for (a) STIC, (b) SEBS and (c) TSEB during the period between 2018 and 2019.

The STIC ET estimates show an advantage performance over those from the PT-JPL model at all the sites (Fig. 3.3). The RMSE of STIC ET is above 100 W m^{-2} at most sites. The positive bias of STIC ET shows the overestimation of PT-JPL ET, which could be due to the weak LST constraint in the PT-JPL model. This is also shown in the difference between the STIC and PT-JPL ET estimates. When the surface wetness is low (with low EC ET), the PT-JPL ET is notably higher than the STIC ET. Especially over shrubland and savanna, the PT-JPL ET is higher than the STIC ET for almost all the samples.

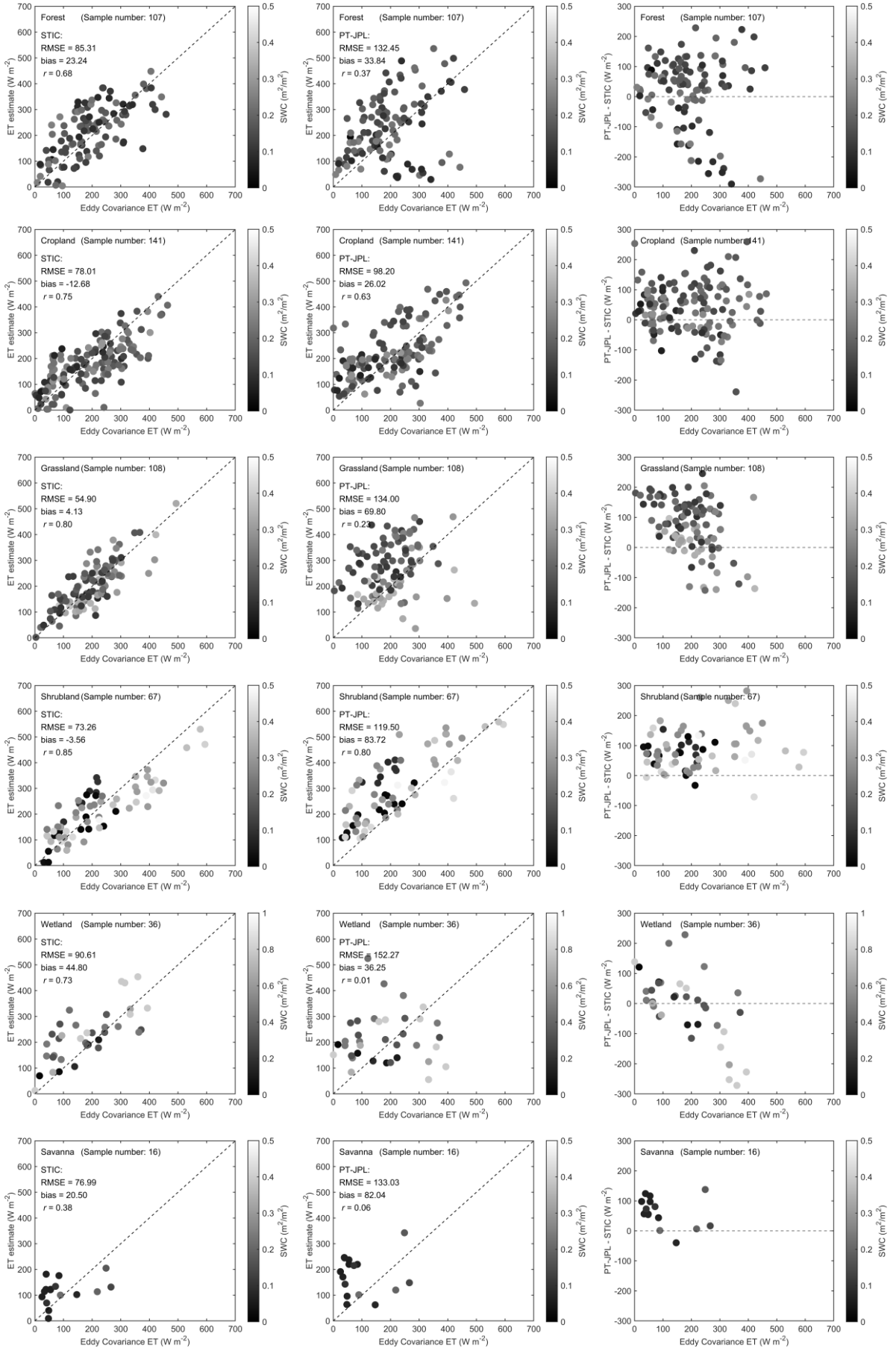
Forest (Sample number: 107)
STIC:
RMSE = 85.31
bias = 23.24
r = 0.68
Forest (Sample number: 107)
PT-JPL:
RMSE = 132.45
bias = 33.84
r = 0.37
Forest (Sample number: 107)
Cropland (Sample number: 141)
STIC:
RMSE = 78.01
bias = -12.68
r = 0.75
Cropland (Sample number: 141)
PT-JPL:
RMSE = 98.20
bias = 26.02
r = 0.63
Cropland (Sample number: 141)
Grassland (Sample number: 108)
STIC:
RMSE = 54.90
bias = 4.13
r = 0.80
Grassland (Sample number: 108)
PT-JPL:
RMSE = 134.00
bias = 69.80
r = 0.23
Grassland (Sample number: 108)
Shrubland (Sample number: 67)
STIC:
RMSE = 73.26
bias = -3.56
r = 0.85
Shrubland (Sample number: 67)
PT-JPL:
RMSE = 119.50
bias = 83.72
r = 0.80
Shrubland (Sample number: 67)
Wetland (Sample number: 36)
STIC:
RMSE = 90.61
bias = 44.80
r = 0.73
Wetland (Sample number: 36)
PT-JPL:
RMSE = 152.27
bias = 36.25
r = 0.01
Wetland (Sample number: 36)
Savanna (Sample number: 16)
STIC:
RMSE = 76.99
bias = 20.50
r = 0.38
Savanna (Sample number: 16)
PT-JPL:
RMSE = 133.03
bias = 82.04
r = 0.06
Savanna (Sample number: 16)
ET estimate (W m-2)
PT-JPL - STIC (W m-2)
Eddy Covariance ET (W m-2)
SWC (m3/m3)

Fig. 3.3 Comparison between the observed ET at eddy covariance sites and instantaneous ET estimates from STIC, SEBS and TSEB for 6 land surface types during the period between 2018−2020. The transparency indicates the aridity level.

The RMSE and bias of STIC ET are ~50 W m^{-2} lower than those of the PT-JPL ET (Fig. 3.4). The correlation with EC measurements is ~0.8 for the STIC ET, while it is below 0.5 for the PT-JPL ET. The better performance of STIC ET is also demonstrated in the Taylor diagram, where the STIC ET is much closer to the observation.

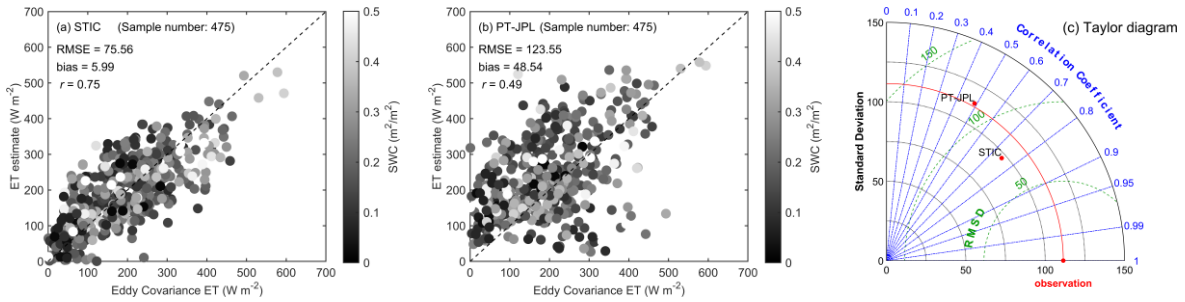

Fig. 3.4 Comparison between the observed ET and instantaneous ET estimates at all the eddy covariance sites for (a) STIC and (b) PT-JPL and (c) Taylor diagram during the period between 2018 and 2020.

4. European Ecostress Hub – Technical realisation

For the reasons presented in the document *European ECOSTRESS Hub Implementation Options Technical Note* (EEH-D2-IOTN), the EEH has been implemented on the Food Security Thematic Exploitation Platform – FS-TEP, according to the principles and the architecture presented in *European ECOSTRESS Hub Technical Specification* (EEH-D3-TS). This document has been updated in order to reflect modifications and adaptations that occurred during the course of the project.

Acknowledgement

The research was carried out at the Luxembourg Institute of Science and Technology, under a contract with the European Space Agency (Contract No. 4000129873/20/I-NS). The authors wish to extend their gratitude to all the scientists involved in the ECOSTRESS mission and ground measurement collection.

Reference

Driemel, A., Augustine, J., Behrens, K., Colle, S., Cox, C., Cuevas-Agulló, E., Denn, F.M., Duprat, T., Fukuda, M., & Grobe, H. (2018). Baseline Surface Radiation Network (BSRN): structure and data description (1992–2017). *Earth System Science Data, 10*, 1491-1501

Freitas, S.C., Trigo, I.F., Bioucas-Dias, J.M., & Gottsche, F.-M. (2009). Quantifying the uncertainty of land surface temperature retrievals from SEVIRI/Meteosat. *IEEE Transactions on Geoscience and Remote Sensing, 48*, 523-534

Göttsche, F.-M., Olesen, F.-S., Trigo, I.F., Bork-Unkelbach, A., & Martin, M.A. (2016). Long term validation of land surface temperature retrieved from MSG/SEVIRI with continuous in-situ measurements in Africa. *Remote Sensing, 8*, 410

Guillevic, P., Göttsche, F., Nickeson, J., Hulley, G., Ghent, D., Yu, Y., Trigo, I., Hook, S., Sobrino, J.A., & Remedios, J. (2018). Land surface temperature product validation best practice protocol. Version 1.1. *Best Practice for Satellite-Derived Land Product Validation, 60*

Hulley, G.C., Göttsche, F.M., Rivera, G., Hook, S.J., Freepartner, R.J., Martin, M.A., Cawse-Nicholson, K., & Johnson, W.R. (2021). Validation and quality assessment of the ECOSTRESS level-2 land surface temperature and emissivity product. *IEEE Transactions on Geoscience and Remote Sensing*

Sobrino, J.A., & Skoković, D. (2016). Permanent stations for calibration/validation of thermal sensors over Spain. *Data, 1*, 10

Trigo, I.F., Ermida, S.L., Martins, J.P.A., Gouveia, C.M., Göttsche, F.-M., & Freitas, S.C. (2021). Validation and consistency assessment of land surface temperature from geostationary and polar orbit platforms: SEVIRI/MSG and AVHRR/Metop. *ISPRS Journal of Photogrammetry and Remote Sensing, 175*, 282-297